LEGIBILITY NOTICE

A major purpose of the Technical Information Center is to provide the broadest dissemination possible of information contained in DOE's Research and Development Reports to business, industry, the academic community, and federal, state and local governments.

Although a small portion of this report is not reproducible, it is being made available to expedite the availability of information on the research discussed herein.

LA-UR- 89-2783

Los Alamos National Laboratory is operated by the University of California for the United States Department of Energy under Contract W-7405-ENG-36

LA-UR--89-2783

DE89 016979

TITLE: KIVA REACTIVE HYDRODYNAMICS CODE APPLIED TO DETONATIONS IN HIGH VACUUM

AUTHOR(S): N. Roy Greiner

DISCLAIMER

Los Alamos National Laboratory
Los Alamos, New Mexico 87545

KIVA REACTIVE HYDRODYNAMICS CODE APPLIED TO DETONATIONS IN HIGH VACUUM

N. ROY GREINER
Chemical and laser Sciences Division
Los Alamos National Laboratory
Los Alamos, NM 87545

ABSTRACT. The KIVA reactive hydrodynamics code has been adapted for modeling detonation hydrodynamics in a high vacuum. Adiabatic cooling rapidly freezes detonation reactions as a result of free expansion into the vacuum. After further expansion, a molecular beam of the products is admitted without disturbance into a drift tube, where the products are analyzed with a mass spectrometer. This paper explains how the model is used for interpretation and design of experiments for detonation chemistry. Modeling of experimental hydrodynamic characterization by laser schlieren imaging and model aided mapping that will link chemical composition data to particular volume elements in the explosive charge are also discussed.

I. Introduction

We have used the KIVA reactive hydrodynamics code (1,2) to provide a computational model of our experiments in frozen detonation chemistry (3-5). By constraining the model with the known essential features of the experiments, we hope to gain insight about the behavior of the experimental system that will aid in interpretation of experimental results and will provide a basis for the design of new experiments.

Briefly, the experiments involve the detonation of condensed explosives in a high vacuum environment (Fig. 1), where the products expand freely and cool adiabatically (to 300 K) in a very short time (2 μs) after the shock arrival. Additional (extensive) expansion after the short freezing step allows the mean free path of the product molecules to increase into the free molecular flow regime so that a molecular beam of the products can be admitted without disturbance to a drift tube through a 1 mm diam skimmer. As the frozen product beam is passing freely down the drift tube, a portion is ionized and its chemical composition is analyzed with a mass spectrometer. Further details are provided in another lecture at this conference (5).

A detailed picture of this process is desired so that the chemical information in the time resolved mass spectral data can be related to the detonation process. The modeling has provided a picture that has proved useful for the highly interactive process of interpretation

and design of experiments. For example, laser-schlieren movies (or sequences of time delayed snapshots) provide information-laden images of the early expansion of the exploding charge. These images cover the time during the passage of the detonation wave through the explosive pellet and the subsequent early expansion while the products are freezing. The modeling suggested the feasibility and usefulness of the experiment, and the successful acquisition of good quality schlieren images stimulated the development of a subroutine to compute expected schlieren images, such as explosive characteristics and starting conditions, while the code was under various constraints. The similarities in the computed and experimental images give confidence in our picture of the hydrodynamic history, and the search for constraints that closely reproduce experimental features leads to insights about the process. Discrepancies between output from the model and observations from experiment stimulate closer examination and refinement of both modeling and experiment.

An example of the application of KIVA is the computed interval of time for the arrival at the mass spectrometer of material from specific (and identifiable) volume elements in the unexploded charge. To the degree that material does not mix between volume elements by processes such as diffusion or turbulence, the time-of-arrival interval can be mapped to specific volume elements, for which a hydrodynamic history is available, with the aid of the model. If this enterprise is successful, we will obtain a sequence of mass spectra for a series of volume elements with model-generated (and experimentally validated) hydrodynamic histories, which include the detonation and quenching processes.

2. The KIVA Code

Our version of the KIVA code has been described (1), and further developments in the code have been made (6). It is an arbitrary Lagrangian-Eulerian (ALE) finite element code (2) for modeling chemically reactive fluids containing condensed droplets. Modifications for modeling free-expansion experiments have been minimal. The principal modifications are the equations of state of the fluids, the reaction models, the schlieren subroutine, the introduction of rezoning and artificial viscosity to smooth shocks, and the selection of input output features. The code provides a file of images of the expanding fluid, including mesh configurations (Figs. 2, 10, 15, and 16); velocity fields (Figs. 3-9, 11-14, and 16); and contours of values for various fluid parameters such as density (Figs. 3-10), pressure, and temperature. Other graphics display parameter values for chosen volume elements as functions of time; among these parameters are density, pressure, temperature, diffusion lengths, mean free path, and measures of reaction progress (Figs. 20-23). Examples are presented below.

3. Modeling

The modeling of detonation, which is a reactive shock, requires a number of tricks to make an assembly of finite elements behave acceptably when the parameters are evaluated and advanced with finite time steps. The two major variations involve artificial viscosity and rezoning, both discussed in the descriptions of KIVA (1) and its predecessor ALE3A. Numerous trials were done to arrive at a compromise between adequate stability and minimal adverse effects on the calculation, but these details will not be elaborated here.

To illustrate our current capability in modeling free-expansion experiments with the KIVA code, we present a selection of results from a single calculation. The parameters chosen were for a nominal case of a right circular cylindrical pellet of RDX (or PETN, approximately) at a loading density of 1.61 g/cm^3. Other details of the calculation are given in Table 1.

TABLE 1. Initial conditions and the governing equations

Charge Geometry:	Right circular cylinder 0.3 cm diam. × 0.3 cm high
Initial Density:	d (g/cm^3) = 1.61
Pressure* of Detonation Products:	P_p (dyne/cm^2) = $2.53 \times 10^{10}\, d^{2.8} + 8.73 \times 10^{9}\, d^{1.4}$
Pressure of Unreacted Explosive:	P_r (dyne/cm^2) = $[7.3 \times 10^{10}\, X + 4.7 \times 10^{11}\,(1 - X)] \times (d - 1.61)$,
where	$X = (2.38 - d/0.77)^{0.4}$
Pressure of Mixture:	P (dyne/cm^2) = $WP_r + (1 - W)P_p$
Temperature:	T (K) = $2287\,[(1 - W)d]^{0.4}$
Burn Rate:	R (1/s) = $2.5 \times 10^{25}\, P^3 + (1 - W)d[\exp(-5000/T)]$
Fraction of Explosive Unreacted:	$W = W_{old}\,[\exp(-R \times dt)]$.
where	W_{old} is the fraction unreacted from the previous time step and dt is the time step.

*10^{11} dyne/cm^2 = 100 kbar = 10 GPa.

Some of the issues to be addressed by the model are time of arrival mapping to location in the charge (Figs. 17 and 18), degree of scrambling of material by turbulence and diffusion (Figs. 20–23), and freezeout or quenching as a function of location in the charge (Figs. 20–23). In effect, what we seek in the model is a plausible (and approximately quantitative) picture of the hydrodynamic history of the detonating material as a function of location in the charge. To validate the model, we compare predictions based on hydrodynamics with observations such as time resolved schlieren images (Figs. 11–15 and 24) and time of arrival profiles (Figs. 17–19). With the modeling results presently in hand, we can assign mass spectra to volume elements with computed hydrodynamic histories.

4. Design of Experiments

We have mentioned the role of modeling in the development and interpretation of the schlieren (Figs. 11-15 and 24) and shadowgraph imaging. Estimates of time and space dependence of fluid densities (Figs. 17-19, for example) have been helpful in designing the new firing chamber, molecular beam drift tube, and mass spectrometer. The scaling of confinement times with charge size and geometry gives estimates of reaction time scales accessible with this technique, which are useful in choosing experiments for particular explosives.

5. Conclusions

Modeling with KIVA is an indispensible adjunct to the free-expansion experiments. Without the modeling, we would have no grasp of the hydrodynamic histories behind the chemical compositions of the frozen reaction products. The model also provides a quantitative mathematical synthesis of the features believed to be important in the overall process of detonation so that the consequences of that synthesis can be foretold, examined, and compared with observation. Discrepancies between model results and experimental observations generate questions that stimulate and direct further investigation.

6. Future Plans

Future plans include a study of chemical reaction models that mimic both observed hydrodynamic phenomena and time dependent chemical composition. It is also desirable to model the leading edge of the expanding products more realistically (compare Figs. 17 and 19). Reduction of artificial numerical contamination of the modeling results is a continuing concern.

We expect that results from our new apparatus (currently under construction) will have considerable influence on future modeling. For instance, if we see significant molecules with a molecular weight higher than the present size limit of 60 amu, their identities and time dependent quantities must be considered when choosing models for computation. The greatly improved mass spectral data acquisition system expands the opportunities for investigating the effects of the many extrinsic parameters, such as those determined by charge microstructure (e.g., crystal structure, crystal size, void size, and void distribution). High speed schlieren and other imaging will afford extensive hydrodynamic characterization of each charge and will provide confidence in linking the chemistry to hydrodynamic history for each shot fired.

Clearly, this technique may have application to a widening variety of systems that involve exploding materials, such as propellants, laser heated materials, electrically heated materials, and materials that are simply shock heated. For example, propellant burn chemistry might be quenched at a desired point in the burn process by firing the propellant in a container sealed with a suitable burstable diaphragm properly aimed at the skimmer. The technique has even been applied to cryogenically prepared samples of energetic materials (7,8).

Acknowledgments

Discussions with my colleagues Norm Blais, Peter O'Rourke, Tony Amsden, Scott Murray, Jack Jacobson, and Frank Harlow were indispensible in the pursuit of this work.

References

1. Amsden, A. A., Ramshaw, J. D., O'Rourke, P. J., and Dukowicz, J. K. (1985), "KIVA: A Computer Program for Two- and Three-Dimensional Fluid Flows with Chemical Reactions and Fuel Sprays," Los Alamos National Laboratory report LA-10245-MS.

2. Hirt, C. W., Amsden, A. A., and Cook, J. L. (1974), "An Arbitrary Lagrangian-Eulerian Computing Method for All Flow Speeds," *J. Comput. Phys.* **14**, 227-253.

3. Greiner, N. R., and Blais, N. C., "Free-Expansion Experiments and Modeling in Detonation: Chemistry and Hydrodynamics on a Laboratory Scale," The Ninth Symposium (International) on Detonation, Portland, Oregon, August 28-September 1, 1989, Preprints, pp. 377-383.

4. Greiner, N. R., "Freely Expanding Detonation Products: Scaling of Rate Processes," 19th International Annual Conference of ICT- Combustion and Detonation Phenomena, Fraunhofer-Institut fuer Chemische Technologie, Karlsruhe, Federal Republic of Germany, June 29-July 1, 1988, pp. 36-1 to 36-13.

5. Blais, N. C., "Detonation Chemistry Studies of Energetic Materials Using Laboratory-Scale Samples," this conference.

6. Amsden, A. A., O'Rourke, P. J., and Butler, T. D. (1989), "KIVA-II: A Computer Program for Chemically Reactive Flows and Sprays," Los Alamos National Laboratory report LA 11560 MS.

7. Greiner, N. R., and Blais, N. C., "Real Time Analysis of the Chemical Products from Shocked Nitric Oxide," 17th International Annual Conference of ICT- Analysis of Propellants and Explosives, Fraunhofer-Institut fuer Treib und Explosivstoffe, Karlsruhe, Federal Republic of Germany, June 25-27, 1986, pp. 33-1to 33-10.

8. Blais, N. C., and Greiner, N. R. (1988), "Real Time Analysis of the Reaction Products of Shocked Solid Nitric Oxide," *J. Energetic Materials* **6**, 255-281.

Figure 1. Schematic of the free-expansion experiment. The skimmer is the cone with the tip missing at the left end of the drift tube. Other features are noted.

Figure 2. Computational mesh at 0.17 μs. K indexes the cells in the Z direction starting with 1 at the bottom of the cylinder, and I indexes the cells in the R direction, starting with 1 next to the cylinder axis. Other cells referred to in the text, along with their (I,K) indices, are A(1,20), B(1,15), C(1,10), and D(10,20). The initial dimensions of the cylinder are Z_{top} = 3.0 mm and R = 1.5 mm. This figure can be compared with Fig. 5, which is also for 0.17 μs. The compressed cells indicate the position of the detonation wavefront.

Figure 3. This and the following figures show the progression of the detonation wave through the 3-mm-diam × 3-mm-high cylindrical pellet with parameters that approximately simulate RDX (or PETN). Initial velocity field and density contours are at 1.5 ns. Vectors originate on cell vertices and length is proportional to velocity. Maximum velocity in the R direction, u, is 0.04 mm/μs and maximum velocity in the Z direction, w, is 0.05 mm/μs. Density is 1.61 g/cm^3 everywhere. The gradients in the initiated cylinder at the bottom are insignificant at this time.

Figure 4. Time = 0.033 μs, Z_{top} = 3.00, u = 1.06 , and w = 1.08. (Here and in the following figures, Z_{top} units will be in mm, velocity units will be in mm/μs and density units will be g/cm^3.) The density contours are based on a logarithmic density scale. Densities on intermediate contours differ by a factor (Q) = 0.966. Maximum density (d_{max}) = 1.830, density on the 11-contour (d11) = 1.768, and density on the 1.-contour (d1.) = 1.344.

Figure 5. Time = 0.085 μs, Z_{top} = 3.00, u = 1.20, w = 1.54, Q = 0.927, d_{max} = 1.995, d11 = 1.847, and d1. = 1.011.

Figure 6. Time = 0.171 μs, Z_{top} = 3.00, u = 1.93, w = 1.81, Q = 0.935, d_{max} = 2.089, d11 = 1.953, and d1. = 1.1395.

Figure 7. Time = 0.306 μs, Z_{top} = 3.00, u = 6.62, w = 2.17, Q = 0.854, d_{max} = 2.161, d11 = 1.844, and d1. = 0.520. The detonation wave has broken out of the bottom half of the charge surface.

Figure 8. Time = 0.447 μs, Z_{top} = 3.14, u = 7.01, w = 5.62, Q = 0.746, d_{max} = 2.174, d11 = 1.622, and d1. = 0.156.

Figure 9. Time = 0.639 μs, Z_{top} = 4.51, u = 7.11, w = 7.45, Q = 0.709, d_{max} = 1.268, d11 = 0.899, and d1. = 0.057. At this time, the detonation wave has broken out of all of the charge surfaces.

Figure 10. Computational mesh and density map. Time = 1.003 μs. Z_{top} = 7.28, Q = 0.675, d_{max} = 0.420, d11 = 0.283, and d1. = 0.012.

Figure 11. Time = 1.003 μs, Z_{top} = 7.28 (same as Fig. 10), u = 7.13, and w = 7.71. This begins a sequence showing computed schlieren-image profiles (right) as contours of deflection angles defined by the schlieren aperture and the Gladstone-Dale constant of the expanding fluid. All schlieren contours overlap in this figure.

Figure 12. Time = 2.000 μs, Z_{top} = 15.00, u = 7.04, and w = 7.74. Schlieren-image contours correspond to different Gladstone-Dale constants for a fixed aperture size. The L contour is that for very complex molecules, and the fifth one from the top is for pure nitrogen gas. The H contour is for a system with a larger aperture than the one used in our experiments. Schlieren contours have the same meaning in Figs. 13-15.

Figure 13. Time = 3.011 μs, Z_{top} = 22.81, u = 6.92, and w = 7.70.

Figure 14. Time = 4.001 μs, Z_{top} = 30.43, u = 6.81, and w = 7.67. Comparison of velocity fields up to this time show that self-similar flow is established by 4 μs.

Figure 15. Time = 5.035 μs, Z_{top} = 39.34. In comparison with Fig. 2, the computational mesh (left) shows distortion caused by the detonation and expansion processes.

Figure 16. Time = 1006.0 μs, Z_{top} = 7.259 m, u = 5.79, and w = 7.14. Comparison of this velocity field with that in Fig. 13 shows the long-time cumulative effects of numerical stability functions on the velocities. Comparison of the computational mesh here with that in Fig. 14 shows the effect of the stability controls on the mesh shape.

Figure 17. Total fluid density vs time-of-arrival at the mass spectrometer located at Z = 1.130 m from the base of the unexploded charge. The points of the sawtooth conveniently mark the times when the leading edge of a new volume element reaches the spectrometer, the earliest being element A in Fig. 1 and the later ones being those shaded cells below A on the cylinder axis. This plot gives information on the mapping of time-of-arrival to volume element, which allows assignment of an observed chemical composition to a particular volume element in the original charge.

Figure 18. Mapping of experimental time-of-arrival data for mass 27 (HCN) to volume elements in the charge. The experimental data (the series of rectangular bars) in arbitrary units, the calculated total fluid density in g/cm^3 (sawtooth curve), and the mapping of time intervals back to volume elements (dotted lines) are shown. This calculation is an earlier one that started with somewhat less realistic conditions than those used in the most recent calculations.

Figure 19. Time of arrival plot for sum of intensities of all masses for RDX. This is the experimental data to be compared with the computed density vs time-of-arrival in Fig. 17.

Figure 20. The first of a set of plots showing parameter values that describe the hydrodynamic history of selected volume elements. This plot is for element A in Fig. 1. The units in this figure and the following ones are centimeter-gram-second units, d = density, P = pressure, DZ = time-integrated diffusion distance, T = temperature in K, MFP = mean-free-path of a nitrogen molecule, TBIM = characteristic reaction time for a bimolecular reaction with arrhenius activation energy of 10 000 cal/mol and arrhenius bimolecular frequency factor of 10^{12} cm^3/mol-s, TUNI = characteristic reaction time for a unimolecular reaction having arrhenius activation energy of 40 000 cal/mol and arrhenius frequency factor of 10^{16}/s. The sharp vertical group of lines marks the arrival of the detonation wave at the cell. Curves at earlier times are minimally meaningful and will not be discussed here. To identify the meaningful part after the detonation wave, we note the markings starting from the topmost and working down: d (solid), P (dotted), DZ (dot-dash), T (solid), MFP (solid), TBIM (dotted), TUNI (solid). The small line segment marks where the reaction-time curves cross the quench line, which is the point where reaction time equals time after initiation. The crossing point is roughly where the reaction quenches. In this case these reactions quench about 0.4 μs after the arrival of the detonation wave. The integrated mean diffusion distance, DZ, is less than 0.1 cm (equivalent to 0.2 μs difference in arrival time) by the time the fluid reaches the mass spectrometer at Z = 1.130 m (at 150-270 μs). This result demonstrates the very small scrambling effect of molecular diffusion.

Figure 21. Hydrodynamic history for Cell B, Fig. 1. Curve identifications are the same as in Fig. 17. Quench comes 1.2 μs after the detonation wave. This cell is expected to be closer to equilibrium than Cell A.

Figure 22. History for Cell C. Quench at 1.6 μs after detonation. This cell should be even closer to equilibrium than Cell B. Cells A, B, and C are among those sampled in the present experimental configuration.

Figure 23. History for Cell D. Quench comes 0.2 μs after detonation, which is faster than in Cell A. This result suggests that the corner is a good place to sample for the most rapidly quenched material.

Figure 24. Comparison of computed and experimental sequences of time-delayed laser-schlieren snapshots for detonation of RDX pellets.

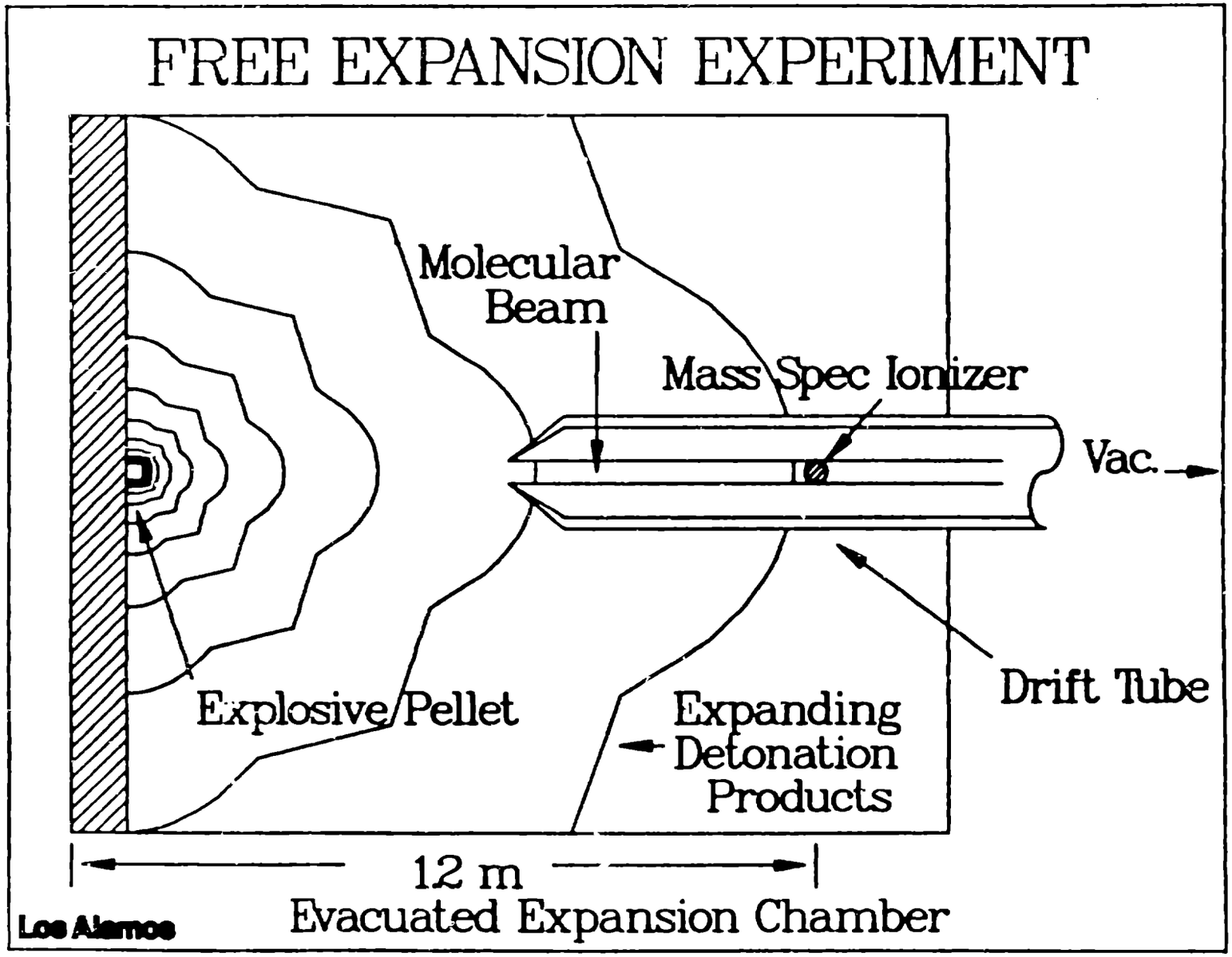
FREE EXPANSION EXPERIMENT
Molecular Beam
Mass Spec Ionizer
Vac.
Drift Tube
Explosive Pellet
Expanding Detonation Products
12 m
Evacuated Expansion Chamber
Los Alamos

Fig 1

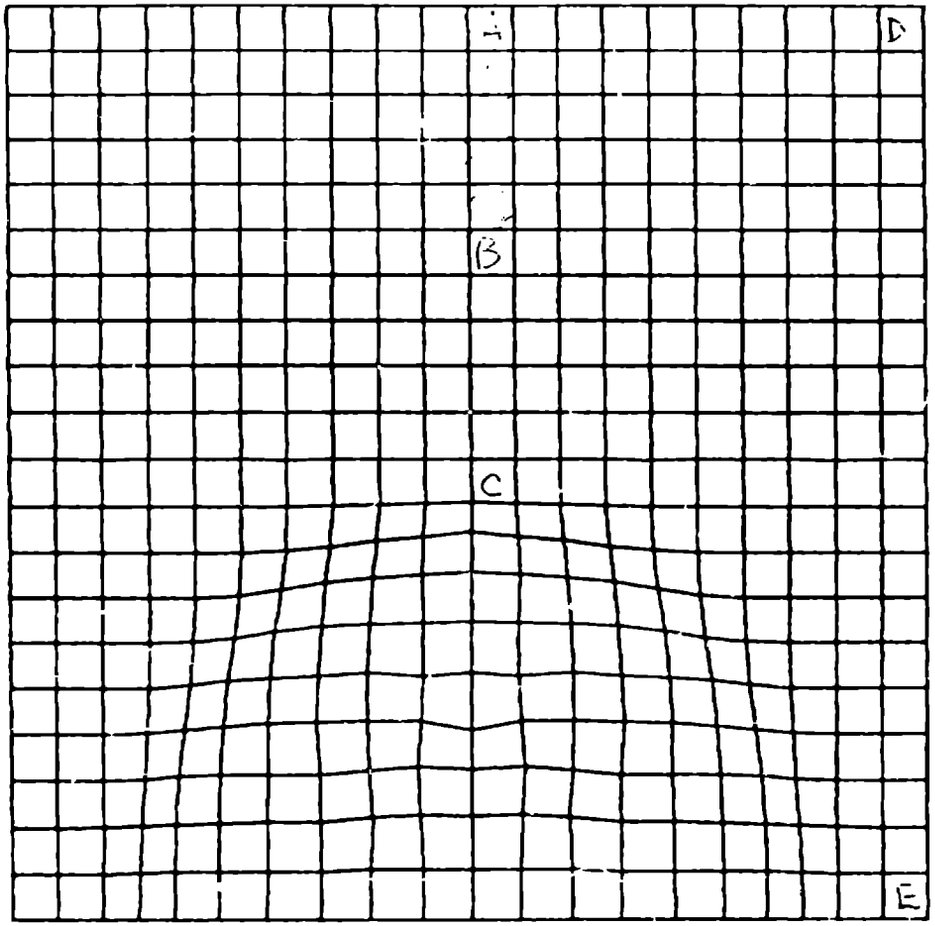

KIVA VERSION DATE: 122387 RUN DATE: 07/20/89 17:23:53
VLMW03(4X4WKIN.ANC4=.05TU.3SUS.CCFLUX CALC.,RK=2.5E-25.PFIND)7/20/89
T= 1.71292E-07 CYCLE 75 ZTOP= 3.00000E-01 RMAX= 1.50000E-01
CROSS-SECTION THROUGH J= 1 (ON THE RIGHT)

Fig 2

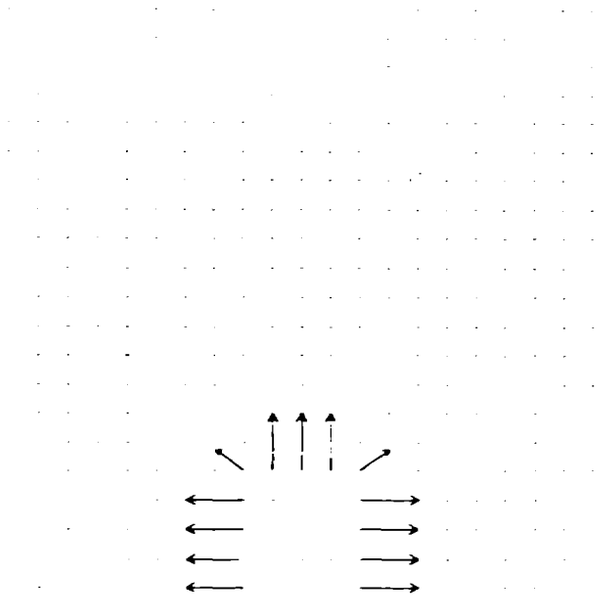

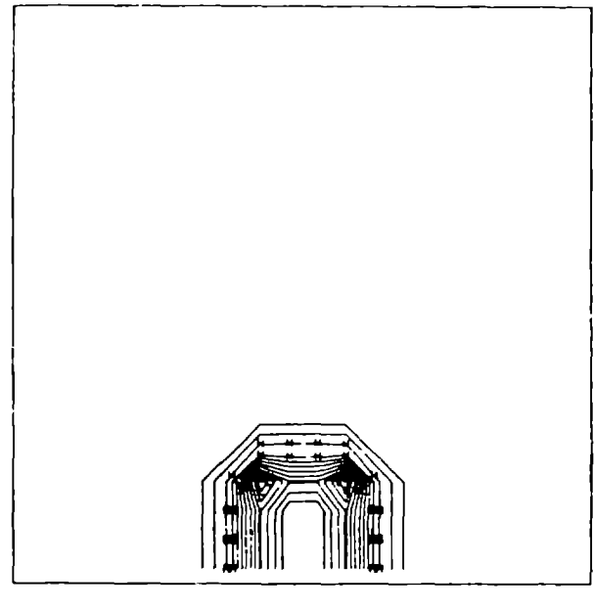

Fig 3

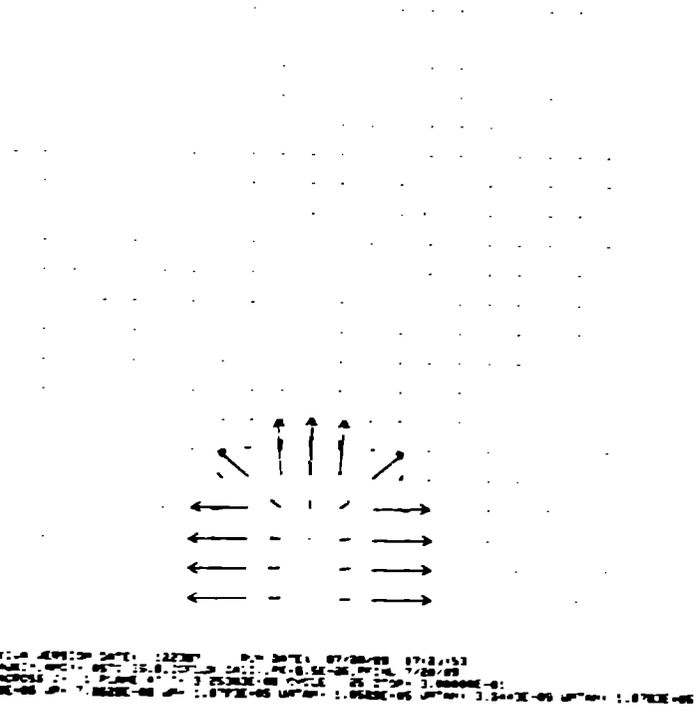

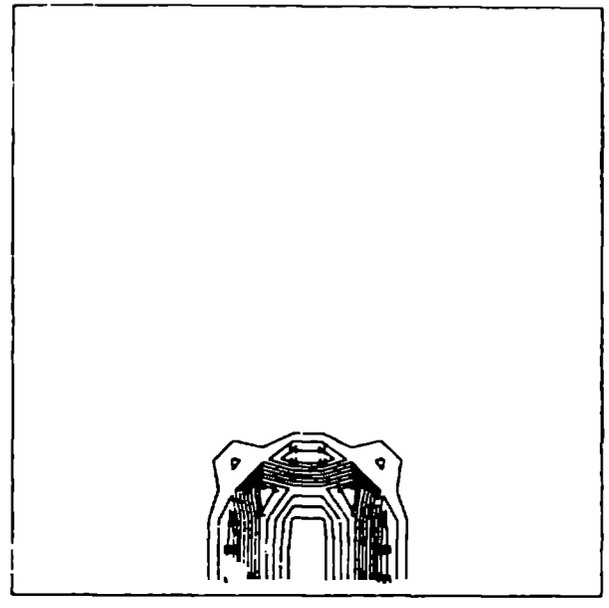

Fig 7

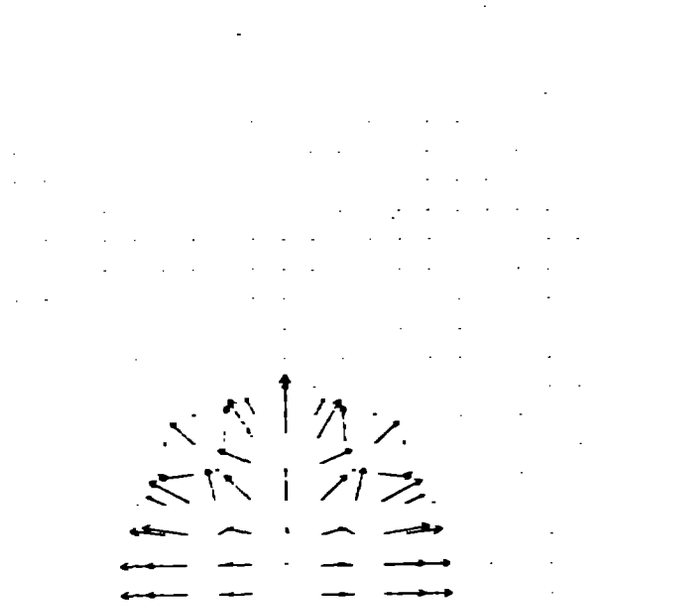

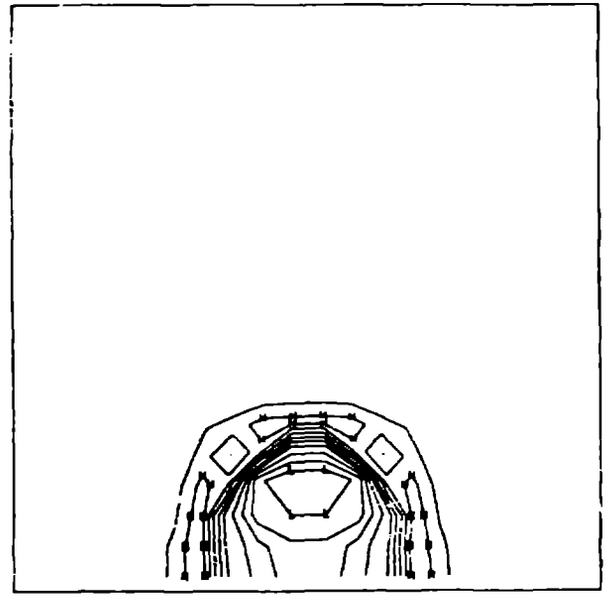

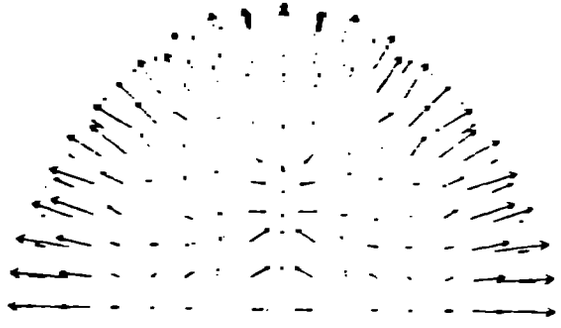

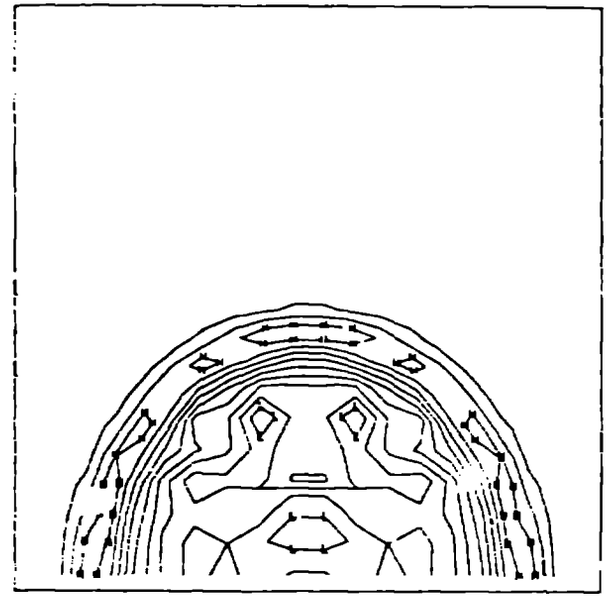

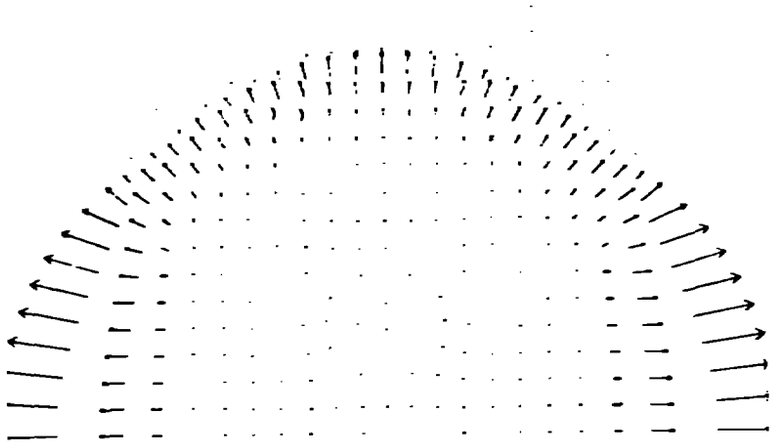

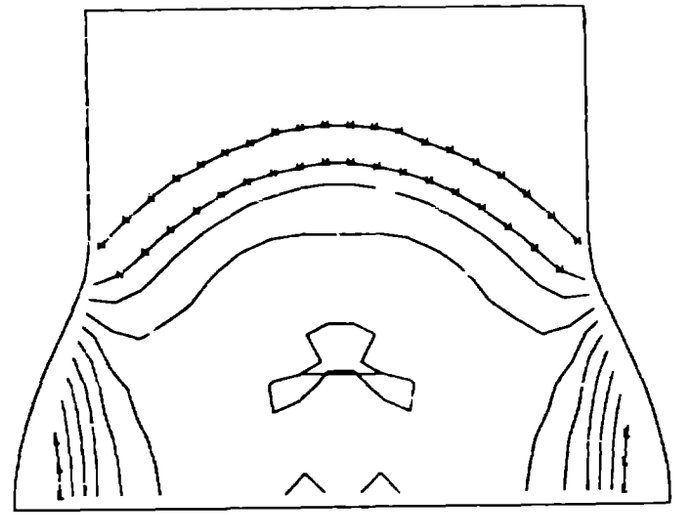

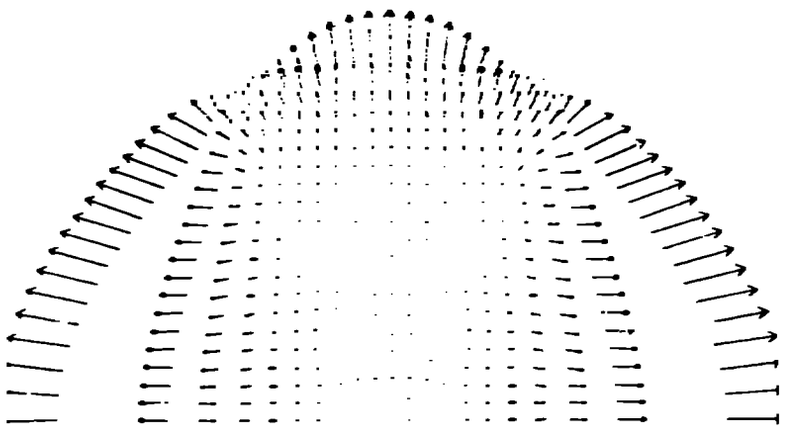

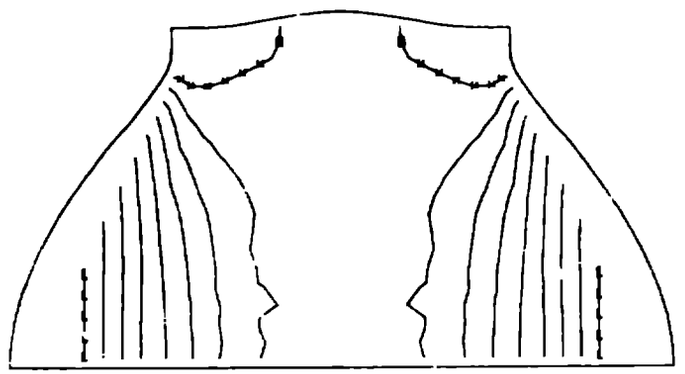

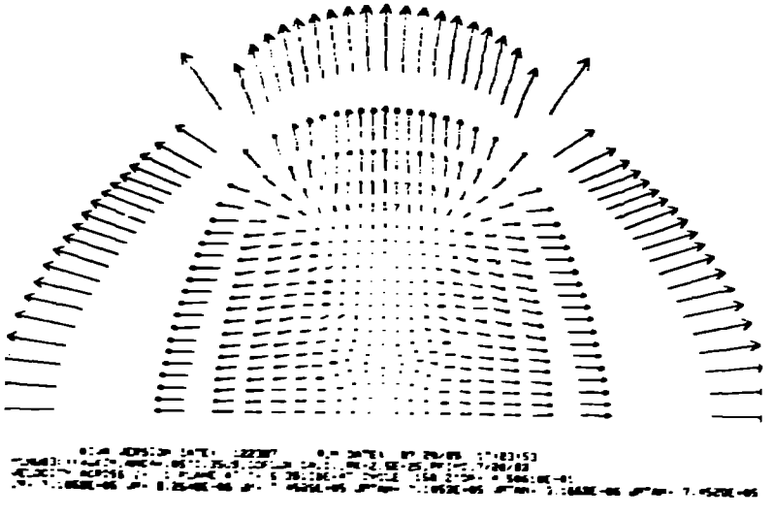

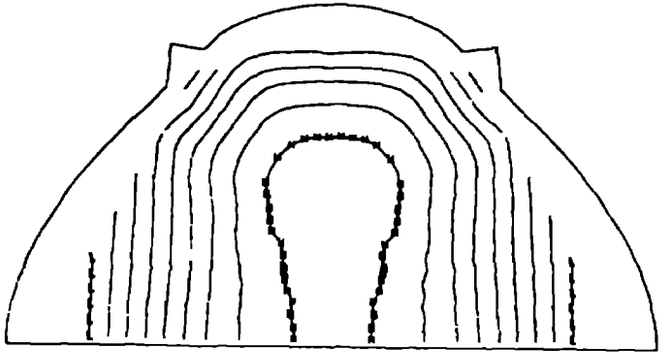

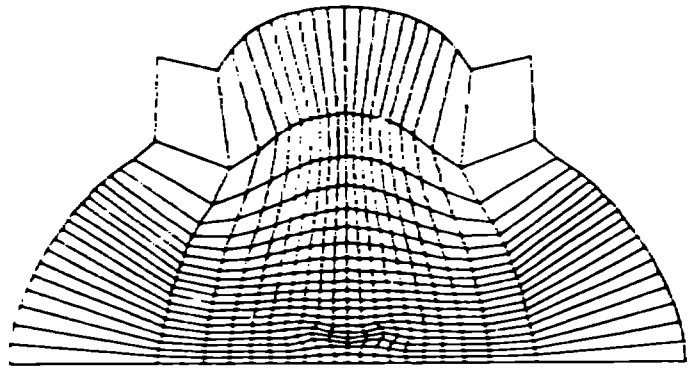

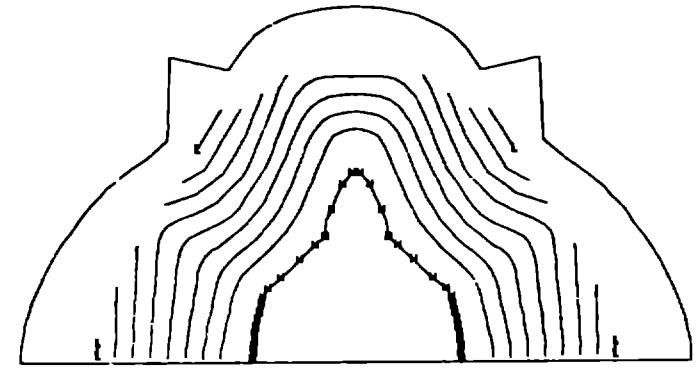

Figure 10

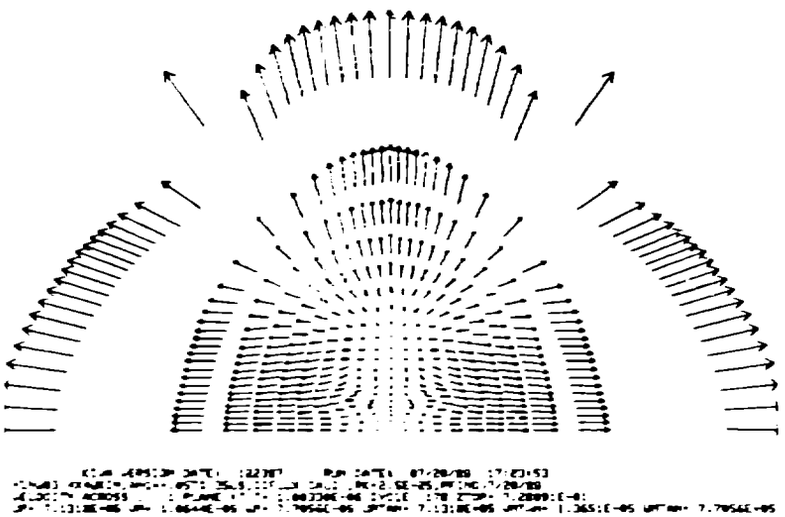

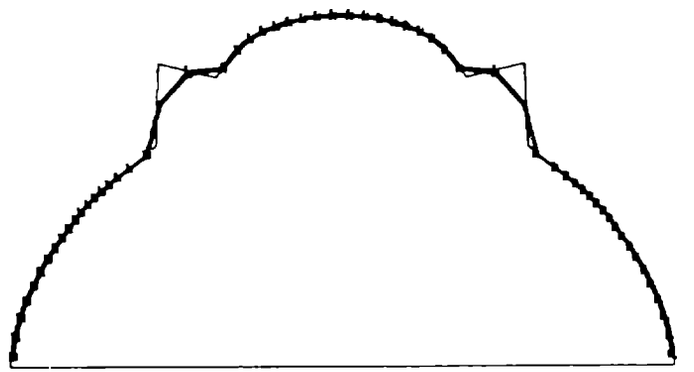

Figure 14

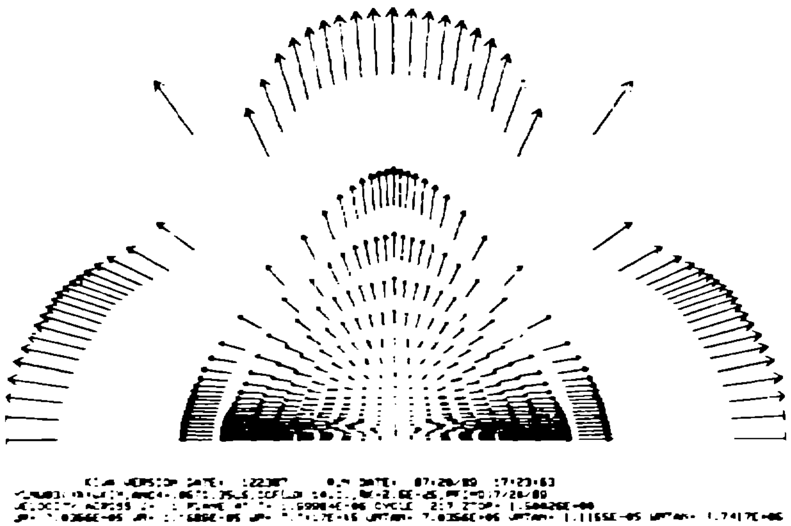
KIVA VERSION DATE
CYCLE 217

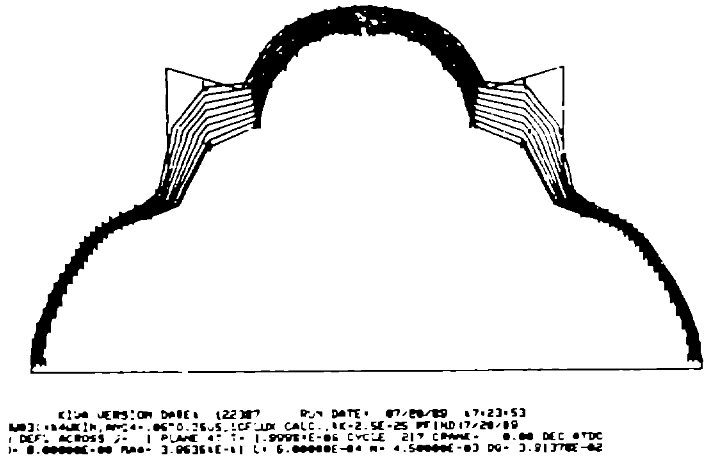
KIVA VERSION DATE
RUN DATE 07/20/89
CALC.
ACROSS
PLANE
CYCLE 217
DEG ATDC

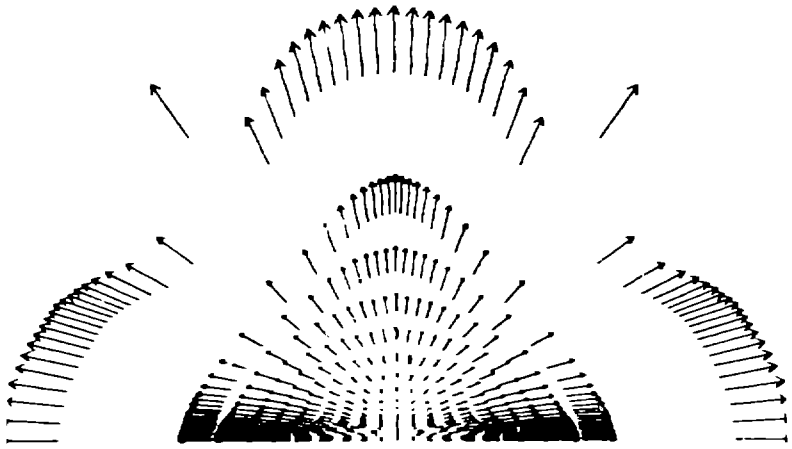

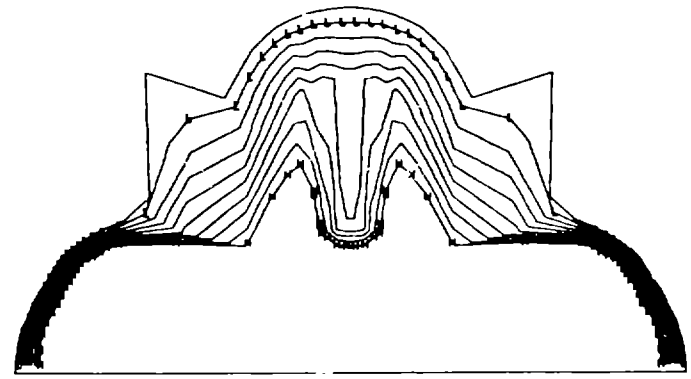

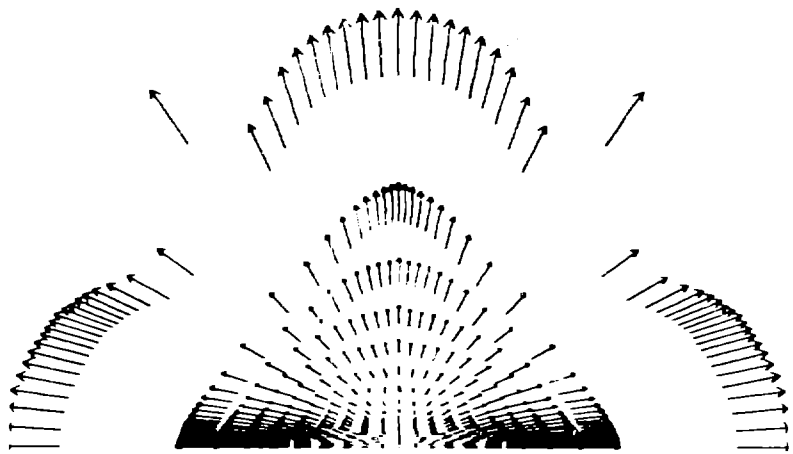

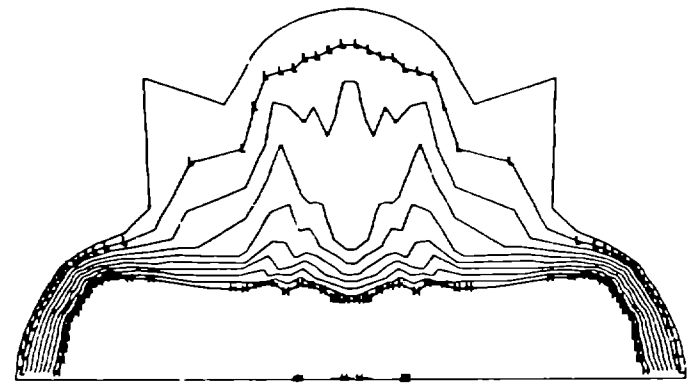

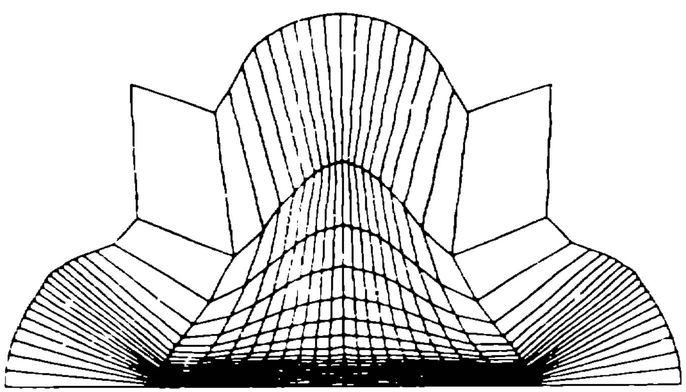

KIVA VERSION DATE= 122387 RUN DATE= 07/20/89 17:23:53
[illegible] 4X4 [illegible] ,.05 [illegible] .35US, [illegible] ,RE=2.5E-25,PF [illegible] 7/20/89
T= 5.03513E-06 CYCLE 266 DTSP= 3.0335[illegible]E-00 PMAX= 3.403[illegible]E-00
CROSS-SECTION THROUGH J= 1 [illegible] THE [illegible]

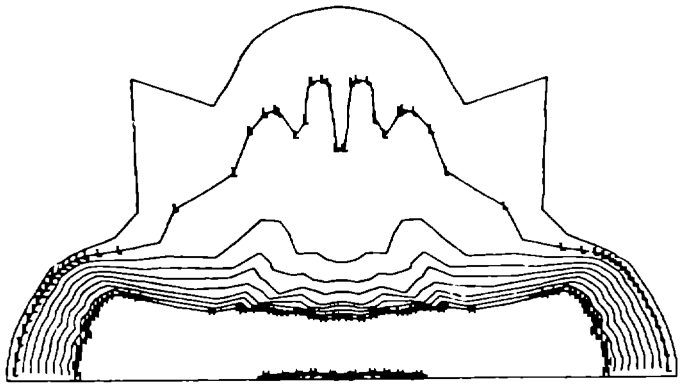

KIVA VERSION DATE= 122387 RUN DATE= 07/20/89 17:23:53
[illegible] 4X4 [illegible] ,.05 [illegible] .35US,CIFLUO CALC.,RE=2.5E-25,PF (HD)7/20/89
C DEF, ACROSS J= 1 PLANE AT T= 5.03513E-06 CYCLE 266 CRANK= [illegible].00 DEG ATDC
N= 0.00000E-00 MAX= 4.59368E-02 L= 5.00000E-04 H= 4.50000E-03 DQ= [illegible].56916E-03

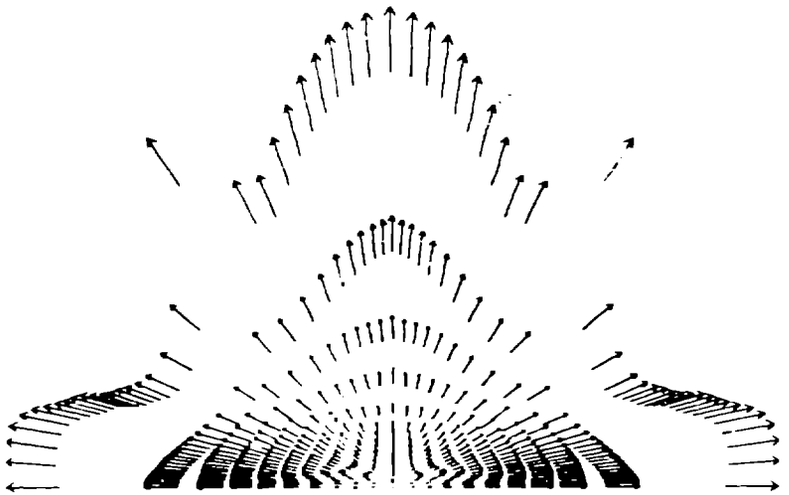

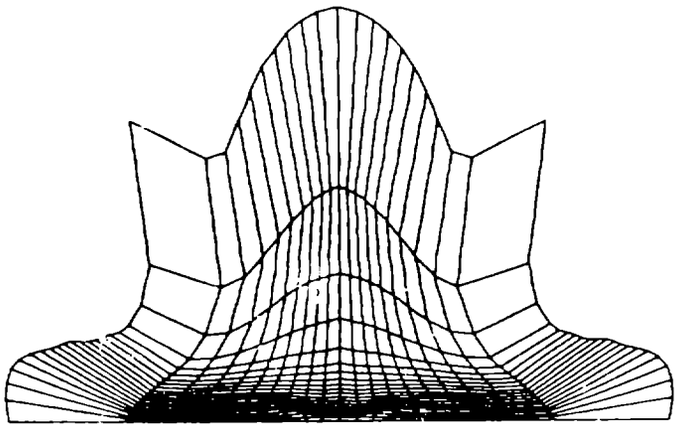

Fig 16

Arrival Time Corresponds to Position in Charge

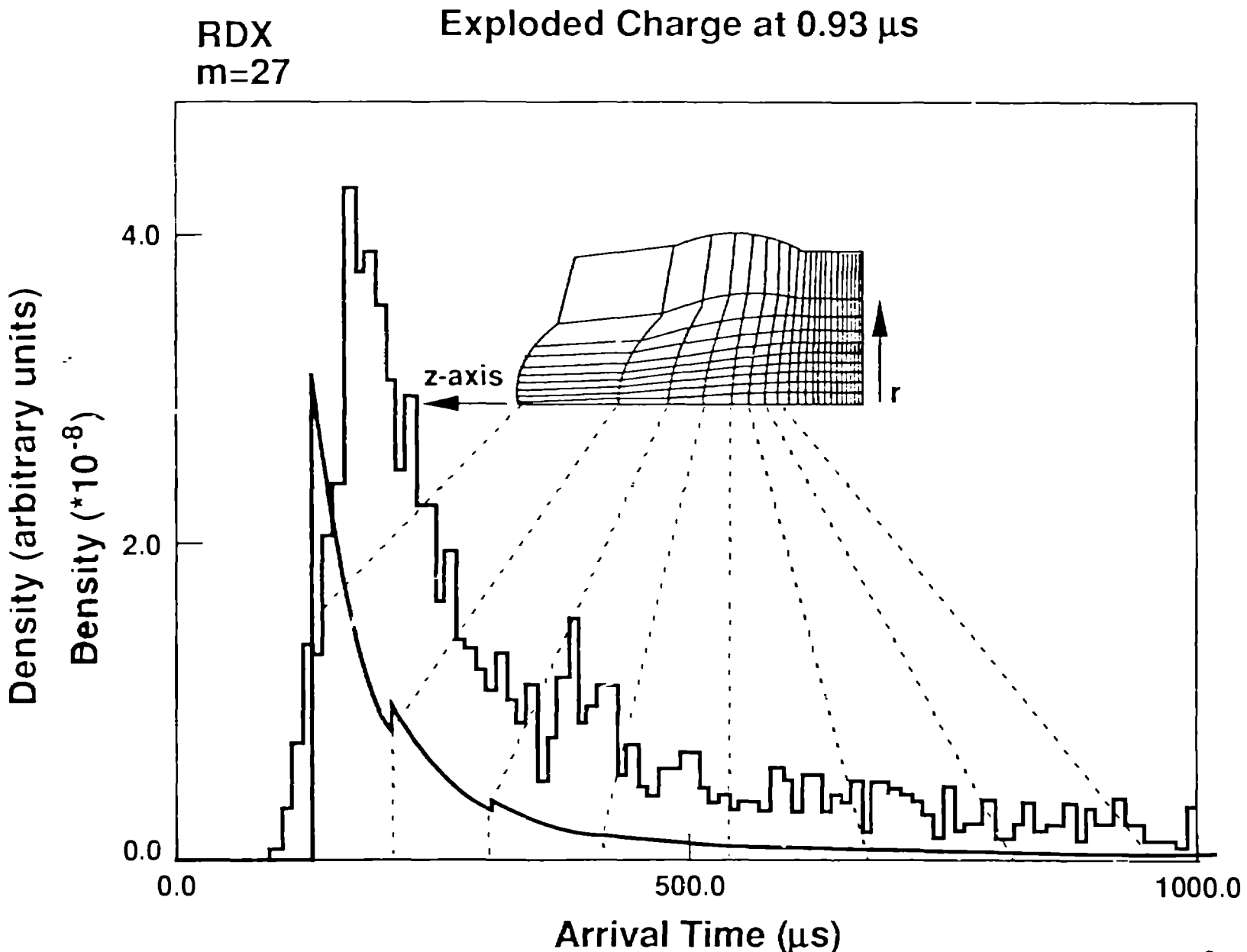

Los Alamos

CLS-88-5704a

21 of 8

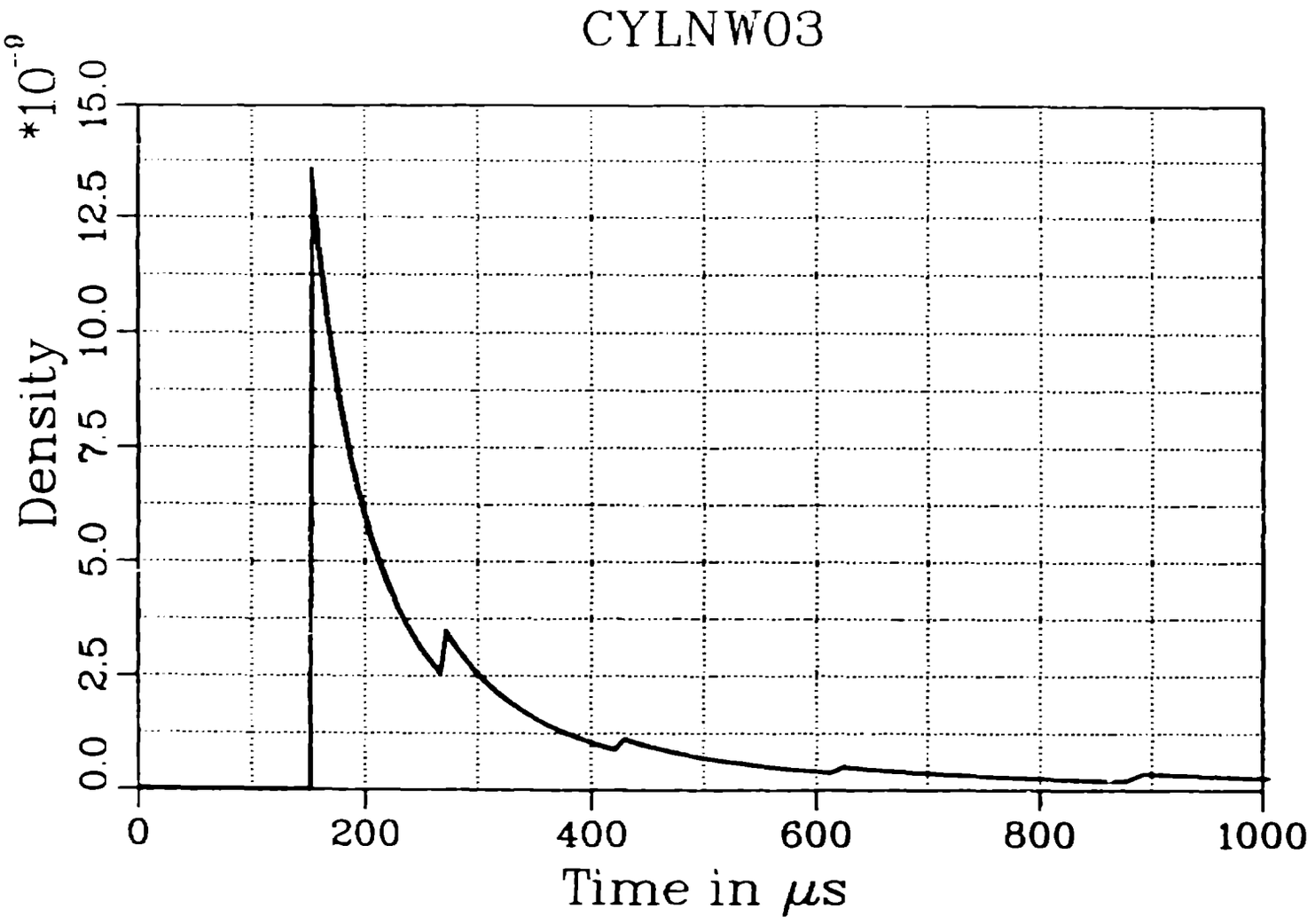
CYLNW03
*10^-9
Density
15.0
12.5
10.0
7.5
5.0
2.5
0.0
0
200
400
600
800
1000
Time in μs

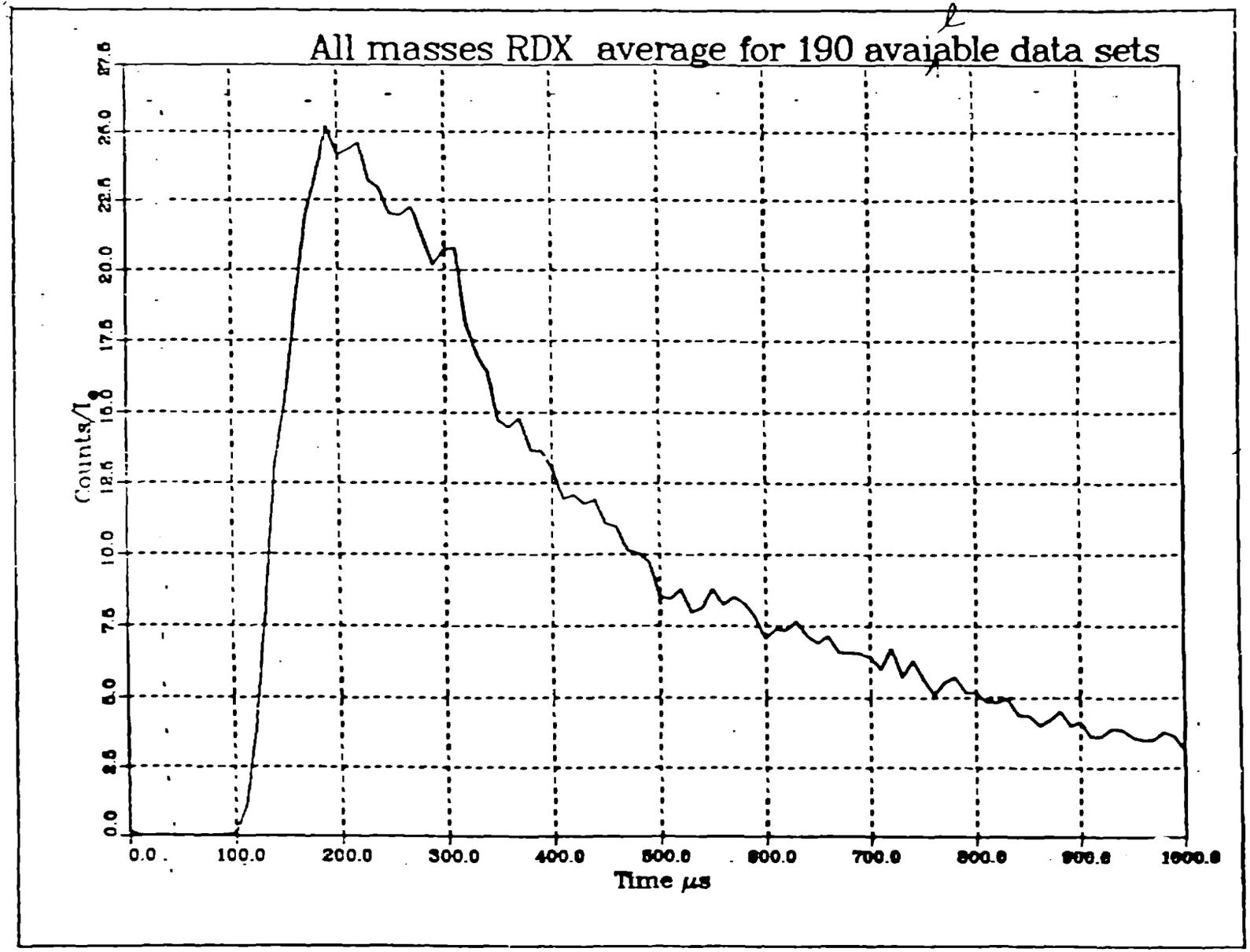
All masses RDX average for 190 avaiable data sets
Counts/1
0.0
2.5
5.0
7.5
10.0
12.5
15.0
17.5
20.0
22.5
25.0
27.5
0.0
100.0
200.0
300.0
400.0
500.0
600.0
700.0
800.0
900.0
1000.0
Time μs

Fig 19

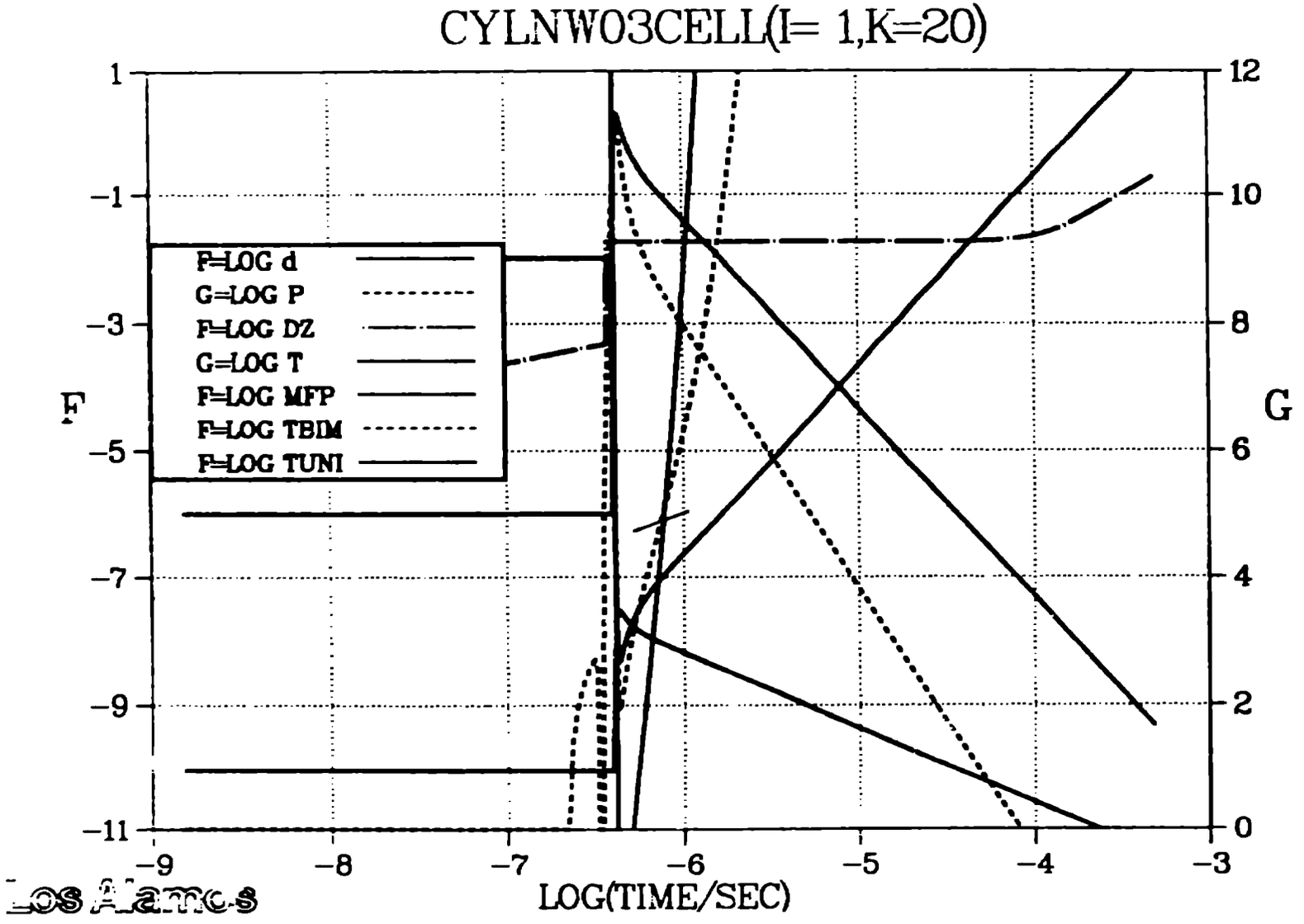
CYLNW03CELL(I= 1,K=20)
F=LOG d
G=LOG P
F=LOG DZ
G=LOG T
F=LOG MFP
F=LOG TBIM
F=LOG TUNI
F
G
LOG(TIME/SEC)
1
-1
-3
-5
-7
-9
-11
12
10
8
6
4
2
0
-9
-8
-7
-6
-5
-4
-3

Los Alamos

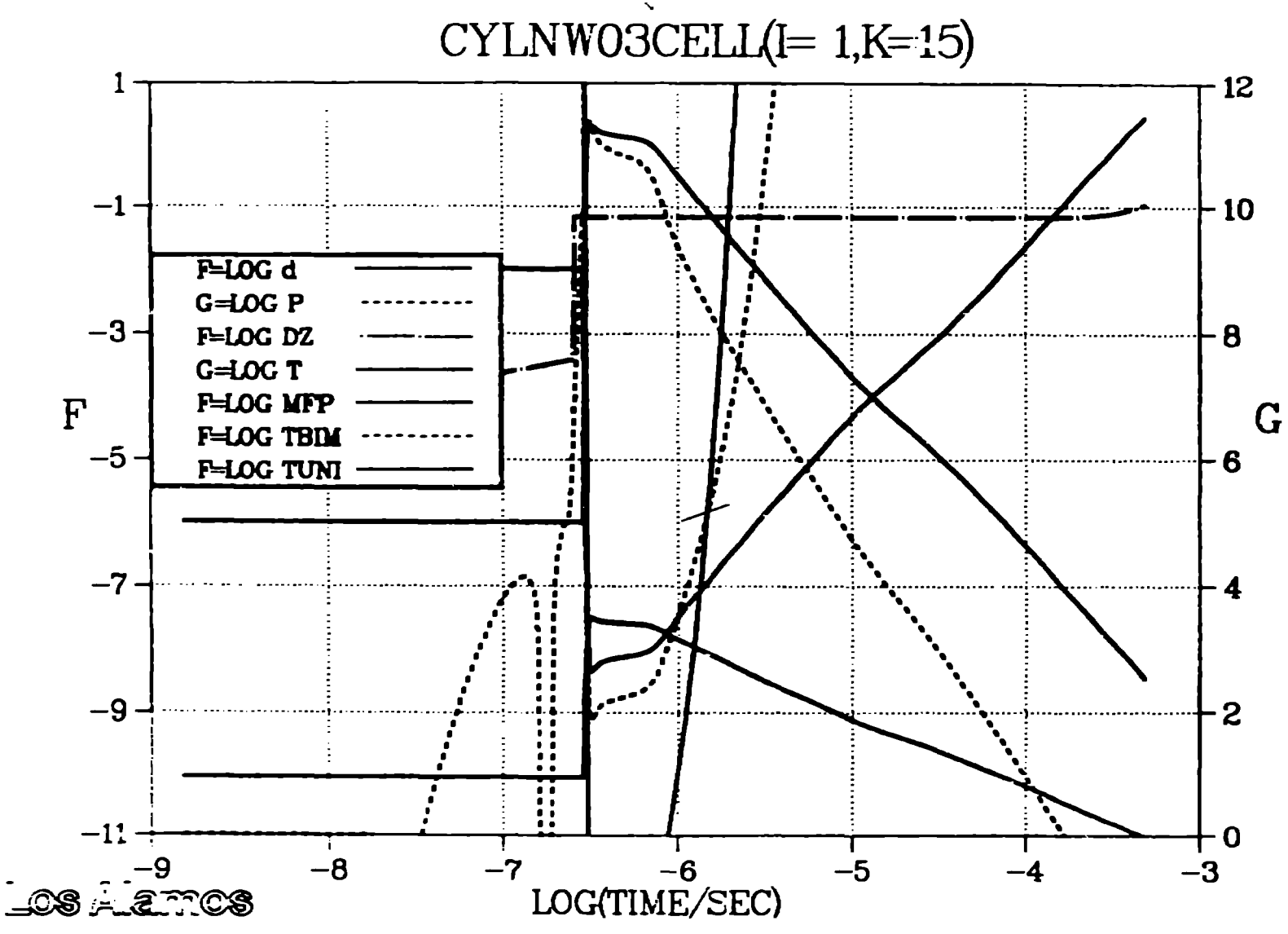
CYLNW03CELL(I= 1,K=15)
F=LOG d
G=LOG P
F=LOG DZ
G=LOG T
F=LOG MFP
F=LOG TBIM
F=LOG TUNI
F
G
LOG(TIME/SEC)
1
-1
-3
-5
-7
-9
-11
12
10
8
6
4
2
0
-9
-8
-7
-6
-5
-4
-3

LOS ALAMOS

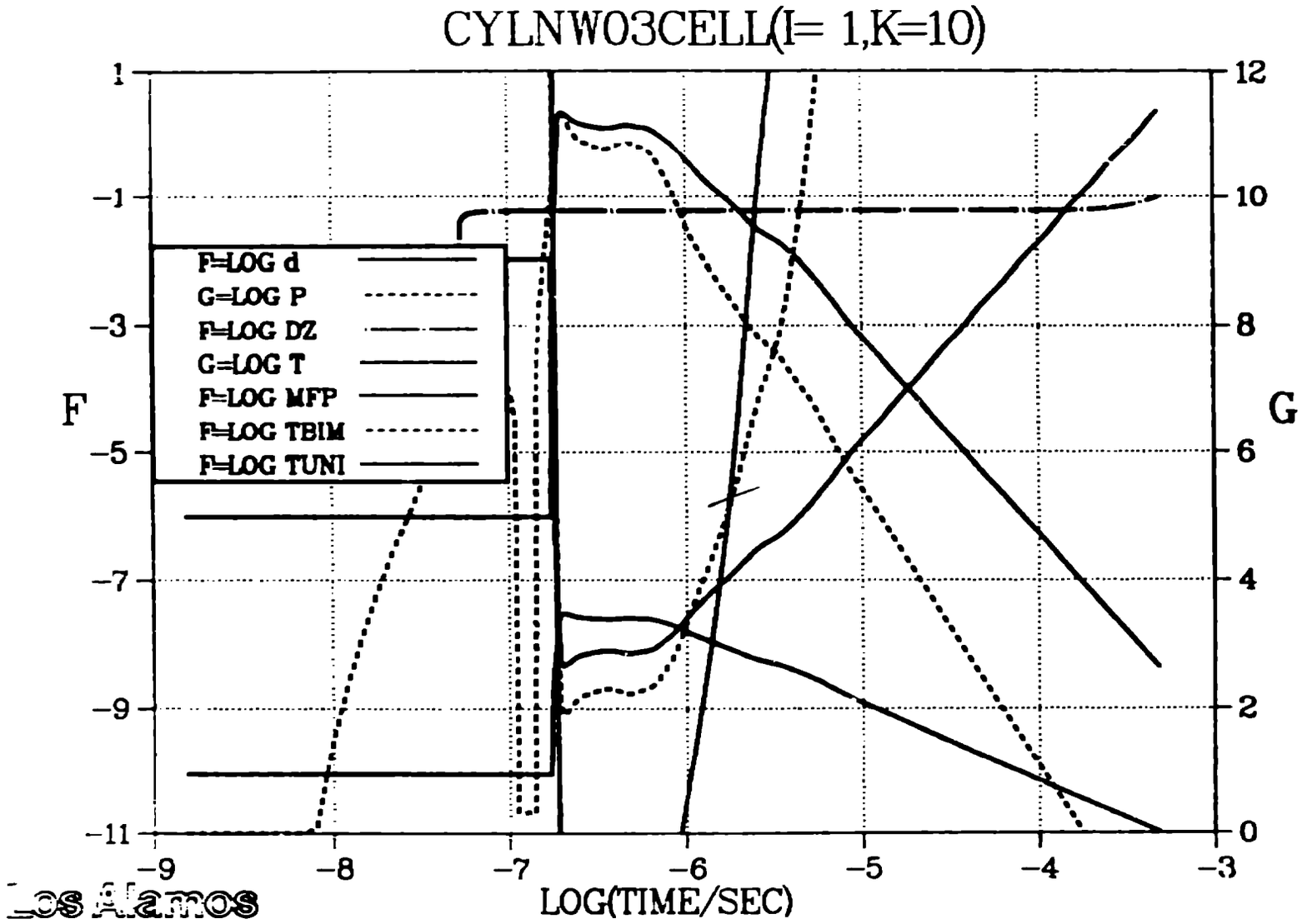
CYLNW03CELL(I= 1,K=10)
F=LOG d
G=LOG P
F=LOG DZ
G=LOG T
F=LOG MFP
F=LOG TBIM
F=LOG TUNI
F
G
LOG(TIME/SEC)
1
-1
-3
-5
-7
-9
-11
12
10
8
6
4
2
0
-9
-8
-7
-6
-5
-4
-3

Los Alamos

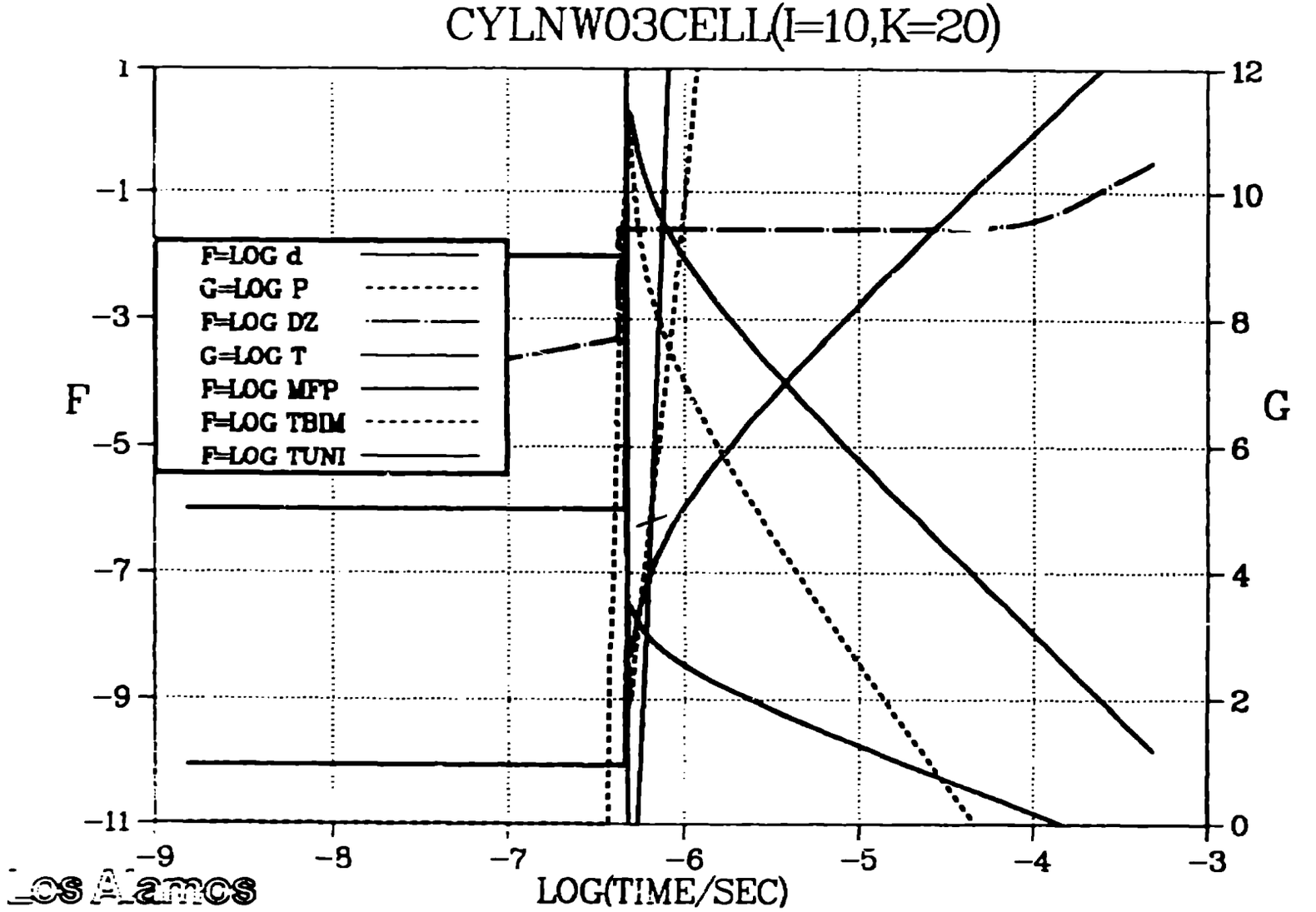
CYLNW03CELL(I=10,K=20)
F=LOG d
G=LOG P
F=LOG DZ
G=LOG T
F=LOG MFP
F=LOG TBDM
F=LOG TUNI
F
G
LOG(TIME/SEC)
1
-1
-3
-5
-7
-9
-11
12
10
8
6
4
2
0
-9
-8
-7
-6
-5
-4
-3

Los Alamos

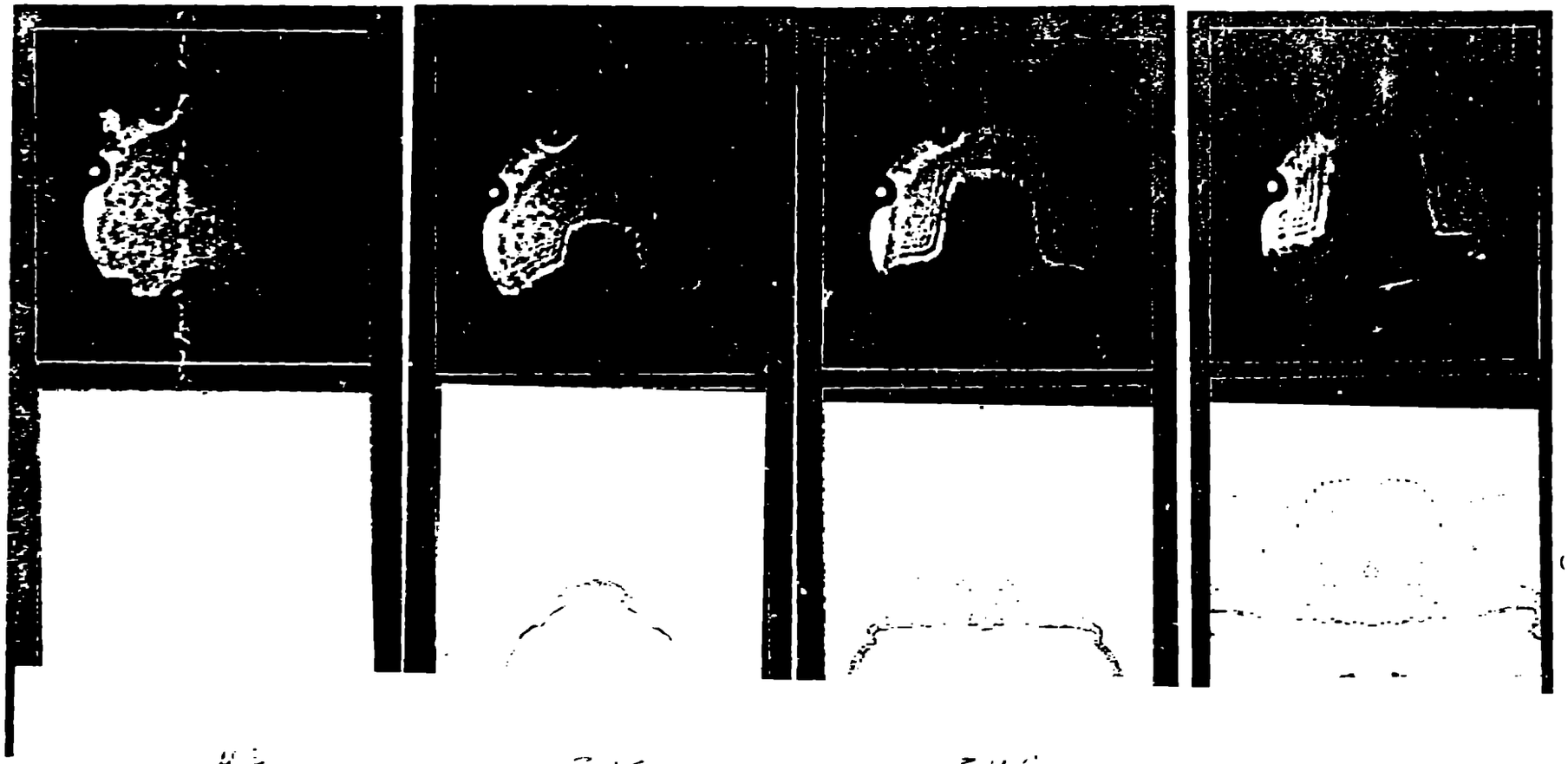
3 US
4 US